

qeirreps: an open-source program for QUANTUM ESPRESSO to compute irreducible representations of Bloch wavefunctions

Akishi Matsugatani^a, Seishiro Ono^a, Yusuke Nomura^b, Haruki Watanabe^a

^a*Department of Applied Physics, University of Tokyo, Tokyo 113-8656, Japan*

^b*RIKEN Center for Emergent Matter Science, 2-1 Hirosawa, Wako, Saitama 351-0198, Japan*

Abstract

Bloch wavefunctions in solids form a representation of crystalline symmetries. Recent studies revealed that symmetry representations in band structure can be used to diagnose the topological properties of weakly interacting materials. In this work, we introduce an open-source program **qeirreps** that computes the representations in a band structure based on the output file of QUANTUM ESPRESSO. Our program also calculates the \mathbb{Z}_4 index, i.e., the sum of inversion parities at all time-reversal invariant momenta, for materials with inversion symmetry. When combined with the symmetry indicator method, this program can be used to explore new topological materials.

Keywords: QUANTUM ESPRESSO; Irreducible representations; Non-symmorphic space groups.

PROGRAM SUMMARY

Program title: qeirreps

Catalogue identifier:

Licensing provisions: GNU General Public Licence 3.0

Programming language: Fortran 90

Computer: any architecture with a Fortran 90 compiler

Operating system: Unix, Linux

RAM: Variable, depends on the complexity of the problem

External routines/libraries used:

- BLAS (<http://www.netlib.org/blas>)
- LAPACK (<http://www.netlib.org/lapack>)

Nature of problem: Irreducible representations of Bloch wavefunctions

Solution method: Linear algebra calculation for Bloch wavefunctions

Running time: 1 min - 1 h (strongly depends on the complexity of the problem)

1. Introduction

One of the main goals in condensed matter physics is to predict the properties of materials of our interest by solving the Schrödinger equation. In practice, this challenging problem is reduced to a manageable one in two ways. The first is to map the interacting system to a free (i.e., noninteracting) electronic system, as is done in the Kohn-Sham density functional theory (DFT) [1]. The other simplification utilizes the symmetry of the system. For example, the lattice translation symmetry of an ideal crystal that is free from impurities or disorders allows us to block-diagonalize the Hamiltonian by switching to the momentum space. The original problem of interacting electrons is thereby transformed into the one within the standard band theory. The

Email address: matsugatani@cmt.t.u-tokyo.ac.jp (Akishi Matsugatani)

Preprint submitted to Elsevier

electronic structure of an enormous number of weakly interacting materials has been successfully computed in this way.

In addition to the lattice translation symmetry, a perfect crystal tends to have other symmetries such as a spatial inversion and a discrete rotation. The set of symmetry operations of a crystal forms a group, called space group. In three dimensions, there are 230 different space groups, and the spatial symmetry of the crystal at work falls into one of them. Crystalline symmetries help us to a better understanding on the electronic band structure. Bloch wavefunctions form a representation of the space group, and the representation puts constraints on how many energy bands degenerate at each momentum and how energy bands at different momenta connect with each other. Furthermore, there has been an increasing number of evidence that the space group representation also informs us of the topological aspects of the Bloch wavefunction.

Since the discovery of the \mathbb{Z}_2 topological insulator [2, 3], topological materials have attracted researchers around the world. In the early stage of the study of topological phases, the focus was on the phases protected by internal symmetries: the time-reversal, the particle-hole, and the chiral symmetry [4, 5, 6, 7, 8, 9, 10, 11, 12, 13, 14, 15, 16, 17, 18]. These pioneering studies were united into the celebrated topological periodic table [19, 20, 21]. They were followed by a large number of studies that take into account the various types of crystalline symmetries [22, 23, 24, 25, 26, 27, 28]. It turned out that there exist various novel topological phases protected by crystalline symmetries, such as mirror Chern insulators [29, 30], higher-order topological insulators [31, 32, 33, 34, 35, 36, 37], and topological semimetals of the Dirac [38] and Weyl [39] type. These topological materials host robust surface states and exhibits unique bulk responses, which could be leveraged for new low-power devices. Therefore, discovering new candidates of topological materials is one of the important tasks both for the fundamental physics and for the application.

At this moment, listing up the full set of topological invariants, for a given symmetry setting, that completely characterize all possible topological phases is still a pending problem. Furthermore, even if we know the mathematical definition of topological invariants, it is sometimes difficult to compute them directly using their definitions [40, 41, 42]. These issues can be resolved with the help of crystalline symmetries. By using the information of the representations of the Bloch wavefunctions at a set of crystalline momenta, it is sometimes possible to judge the topology encoded in the Bloch wavefunctions quite easily. The prototypical example is the Fu-Kane formula [9], which determines the \mathbb{Z}_2 invariant based on the inversion parities. Recently, this idea has been extended to a wider class of topological (crystalline) insulators and semimetals in all 230 space groups [43]. The usefulness of this extended method, called “symmetry indicators,” in the search for realistic topological materials was clearly demonstrated by the recent comprehensive survey of topological materials among existing databases of inorganic substances [44, 45, 46, 47, 48]. As a result of this survey, thousands of candidates of topological (crystalline) insulators and semimetals have been identified. The theory of symmetry indicators has also been extended to magnetic space groups [49] and superconductors [50, 51, 52, 53, 54, 55], and further investigation of topological magnetic materials and superconductors is awaiting us.

Having in mind these applications, it is evidently important to make it possible to automatically compute irreducible representations of Bloch wavefunctions by using DFT. Although the authors of Refs. [44, 45, 46, 47, 48, 56] implemented this function for WIEN2k [57] and VASP [58], these softwares require paid licenses. In contrast, for the QUANTUM ESPRESSO [59, 60], which is a free, open-source package, the existing program can handle only one type of space groups, called “symmorphic” space groups, and does not work for the other type, called “non-symmorphic.” Given this situation, we develop an open-source code, named `qeirreps`, that works equally for symmorphic and non-symmorphic space groups. This would allow everyone to compute the band structure and determine the irreducible representations by themselves, and when combined with the method of symmetry-indicator, would accelerate our search of novel topological materials like topological superconductors.

The rest of this paper is organized as follows. In Sec. 2, we briefly review the theoretical background of space groups and their representations. In Sec. 3, we explain the installation and usage of `qeirreps`. After providing some examples: bismuth, silicon, and PbPt_3 in Sec. 4, we conclude in Sec. 5.

2. Theoretical background

We start with reviewing the basics of space groups and their representations.

2.1. Space group action on the real and momentum space

Let us consider a space group \mathcal{G} . An element $g \in \mathcal{G}$ moves $\mathbf{x} \in \mathbb{R}^3$ to

$$g(\mathbf{x}) = p_g \mathbf{x} + \mathbf{t}_g \in \mathbb{R}^3, \quad (1)$$

where $p_g \in O(3)$ represents the point group part and $\mathbf{t}_g \in \mathbb{R}^3$ represents the translation part of g . The product of two elements $g \in \mathcal{G}$ and $g' \in \mathcal{G}$ is defined by

$$p_{gg'} = p_g p_{g'}, \quad \mathbf{t}_{gg'} = p_g \mathbf{t}_{g'} + \mathbf{t}_g. \quad (2)$$

In general, \mathbf{t}_g is not necessarily a lattice vector. If we can choose the origin of \mathbf{x} in such a way that \mathbf{t}_g becomes a lattice vector simultaneously for all $\forall g \in \mathcal{G}$, the space group is symmmorphic; otherwise, it is nonsymmorphic. Nonsymmorphic space groups typically contain either screw axes or glide planes.

A space group \mathcal{G} always has a subgroup T composed of lattice translations. An element $T_{\mathbf{R}}$ of T can be characterized by a lattice vector \mathbf{R} . We introduce the wavevector \mathbf{k} through the representation of $T_{\mathbf{R}}$:

$$U_{\mathbf{k}}(T_{\mathbf{R}}) = e^{-i\mathbf{k} \cdot \mathbf{R}}. \quad (3)$$

An element $g \in \mathcal{G}$ changes \mathbf{k} to $g(\mathbf{k}) = p_g \mathbf{k}$. We say \mathbf{k} is invariant under g when $g(\mathbf{k}) = \mathbf{k} + \mathbf{G}$ with a reciprocal lattice vector \mathbf{G} . For each \mathbf{k} , the set of $g \in \mathcal{G}$ that leaves \mathbf{k} invariant, i.e., $\{h \in \mathcal{G} \mid h(\mathbf{k}) = \mathbf{k} + \mathbf{G}\}$, forms a subgroup of \mathcal{G} called the little group $\mathcal{G}_{\mathbf{k}}$.

2.2. Crystalline symmetries of band structures

Suppose that the single-particle Hamiltonian in momentum space satisfies

$$U_{\mathbf{k}}(g)H_{\mathbf{k}} = H_{p_g \mathbf{k}}U_{\mathbf{k}}(g). \quad (4)$$

Here unitary matrices $U_{\mathbf{k}}(g)$ form a projective representation of \mathcal{G} . That is, they satisfy

$$U_{g' \mathbf{k}}(g)U_{\mathbf{k}}(g') = \omega^{\text{sp}}(g, g')U_{\mathbf{k}}(gg'), \quad (5)$$

where $\omega^{\text{sp}}(g, g') = \pm 1$ is the projective factor originated from the spin of electrons. For spin-rotation invariant systems, $\omega^{\text{sp}}(g, g')$ can be chosen 1 by neglecting the spin degree of freedom.

The single-particle Hamiltonian $H_{\mathbf{k}}$ can be diagonalized as

$$H_{\mathbf{k}} = \Psi_{\mathbf{k}} \begin{pmatrix} \epsilon_{\mathbf{k}1} \mathbb{1}_{\alpha_1} & 0 & \cdots & 0 \\ 0 & \epsilon_{\mathbf{k}2} \mathbb{1}_{\alpha_2} & \cdots & 0 \\ \vdots & \vdots & \ddots & \cdots \\ 0 & 0 & \cdots & \epsilon_{\mathbf{k}M_{\mathbf{k}}} \mathbb{1}_{\alpha_{M_{\mathbf{k}}}} \end{pmatrix} \Psi_{\mathbf{k}}^\dagger, \quad (6)$$

where $\epsilon_{\mathbf{k}n}$ is the n -th eigenenergy of $H_{\mathbf{k}}$, and $\Psi_{\mathbf{k}}$ is composed of all eigenvectors of $H_{\mathbf{k}}$. When h is an element of $\mathcal{G}_{\mathbf{k}}$, $U_{\mathbf{k}}(h)$ can also be block-diagonalized by $\Psi_{\mathbf{k}}$ into irreducible representations $U_{\mathbf{k}}^\alpha(h)$:

$$U_{\mathbf{k}}(h) = \Psi_{\mathbf{k}} \begin{pmatrix} U_{\mathbf{k}}^{\alpha_1}(h) & 0 & \cdots & 0 \\ 0 & U_{\mathbf{k}}^{\alpha_2}(h) & \cdots & 0 \\ \vdots & \vdots & \ddots & \cdots \\ 0 & 0 & \cdots & U_{\mathbf{k}}^{\alpha_{M_{\mathbf{k}}}}(h) \end{pmatrix} \Psi_{\mathbf{k}}^\dagger \quad (\forall h \in \mathcal{G}_{\mathbf{k}}), \quad (7)$$

Although the specific representation $U_{\mathbf{k}}^{\alpha_n}(h)$ depends on the detailed choice of $\Psi_{\mathbf{k}}$, its character

$$\chi_{\mathbf{k}}^{\alpha_n}(h) = \text{tr}[U_{\mathbf{k}}^{\alpha_n}(h)] \quad (8)$$

is basis independent. The output of our program is the list of characters $\chi_{\mathbf{k}}^{\alpha_n}(h)$ for each the energy level $\epsilon_{\mathbf{k}n}$ and high-symmetry point \mathbf{k} .

Since $\mathcal{G}_{\mathbf{k}}$ is an infinite group due to its translation subgroup T , sometimes the finite group $\mathcal{G}_{\mathbf{k}}/T$, called “little co-group [61],” is discussed instead. Irreducible representations of $\mathcal{G}_{\mathbf{k}}/T$ and $\mathcal{G}_{\mathbf{k}}$ are related to each other by a simple rule, and one can convert one to the other easily. Note that the output of our program is the character of representations of $\mathcal{G}_{\mathbf{k}}$, not $\mathcal{G}_{\mathbf{k}}/T$, and one should not confuse them.

2.3. Application to symmetry indicators

The characters $\chi_{\mathbf{k}}^{\alpha}(h)$ in the output of our program can be converted to integers $\{n_{\mathbf{k}}^{\alpha}\}$ that count irreducible representations $U_{\mathbf{k}}^{\alpha}(h)$ appearing in the occupied bands at each high-symmetry point \mathbf{k} . These integers can be used, for example, to diagnose the topological indices of band insulators through the method of symmetry indicators [43, 62]. Formulas of topological indices in terms of $\{n_{\mathbf{k}}^{\alpha}\}$ are provided in Refs. [63, 64, 65, 50].

For the user’s convenience, we implemented the function that automatically computes the \mathbb{Z}_4 index as the sum of the inversion parities of all occupied bands at all the time-reversal invariant momenta (TRIMs). The \mathbb{Z}_4 index can detect not only strong topological insulators but also topological crystalline insulators such as mirror Chern insulators or higher-order topological insulators [64, 65]. See Sec. 4.1 for an example.

Other symmetry indicators can also be computed in the same way using the output of our program. We discuss several examples in Sec. 4.3.

2.4. Conventions

Let us summarize our conventions that are necessary to compare the output of our program with that of others. There are three sources of ambiguities that affect the $U(1)$ phase of the representation $U_{\mathbf{k}}^{\alpha}(h)$: (i) the choice of representatives of \mathcal{G} , (ii) the choice of the coordinates, and (iii) the choice of spin rotation matrices. Readers not interested in the details can skip to Sec. 3.

2.4.1. The choice of representatives of \mathcal{G}

Although the number of elements of \mathcal{G} is infinite because of its translation subgroup, in the actual calculation, it is sufficient to discuss a finite number of elements by choosing one $g \in \mathcal{G}$ for each p_g . This is because, if g' differs from g by its translation part (i.e., $p_{g'} = p_g$ and $\mathbf{t}_{g'} = \mathbf{t}_g + \mathbf{R}$ for a lattice vector \mathbf{R}), the little-group representation of g' is simply given by $U_{\mathbf{k}}(g') = U_{\mathbf{k}}(g)e^{-i\mathbf{k}\cdot\mathbf{R}}$. The choice of g ’s is not unique, and in our program, they are automatically selected by QUANTUM ESPRESSO based on the input file. The chosen elements of \mathcal{G} are stored in our output files: the list of p_g ’s is in `pg.dat` and the list of the corresponding \mathbf{t}_g ’s is in `tg.dat`.

2.4.2. The choice of the coordinates

When using QUANTUM ESPRESSO, one needs to prepare an input file that contains the information of the coordinates of atomic positions. In QUANTUM ESPRESSO, the fixed point of point group symmetries is always set to $(0,0,0)$, and the input file must be carefully prepared. For a given material, even after fixing the symmetry operation, there can still be multiple choices of the coordinates, and the irreducible representations can in general be affected by this choice. In our examples discussed in Sec. 4, the information of the chosen coordinates is stored in the input file named `*.scf.in`.

To see this subtlety through a simple example, let us consider the inversion symmetric 1D system illustrated in Fig. 1. In this model, there are two atoms A and B in a unit cell. In the panel (a), the atom A is placed at the origin and the coordinate of the atom B is $x = \frac{1}{2}$. In the panel (b), the atom B is placed at the origin and the coordinate of the atom A is $x = \frac{1}{2}$. This is the ambiguity of the coordinates mentioned above. In both cases, the inversion symmetry is about the origin $x = 0$, but the atom at the fixed point is different. This means that the inversion in (a) and that in (b) are physically different operations. As a consequence, their representations are not the same and are related by $U_{k_x}^{\alpha}(I)^{(a)} = e^{ik_x}U_{k_x}^{\alpha}(I)^{(b)}$.

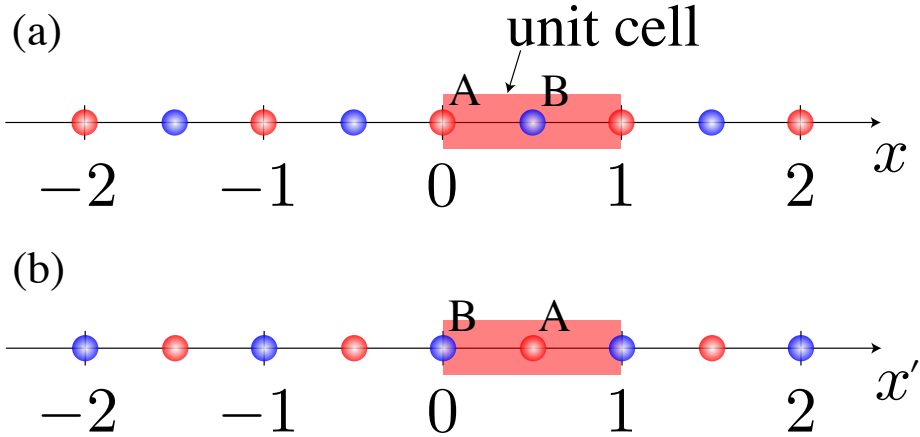


Figure 1: Two choices of the coordinate for an inversion symmetric 1D system composed of two atoms A and B in each unit cell. The origin of the coordinate is at the atom A in the panel (a), while it is at the atom B in the panel (b).

2.4.3. The choice of the spin rotation

As is well-known, the correspondence between a point group $p_g \in O(3)$ and the spin rotation $p_g^{\text{sp}} \in SU(2)$ has a sign ambiguity. Namely, when p_g^{sp} denotes a spin rotation corresponding to the point group p_g , $-p_g^{\text{sp}}$ is also an equally valid choice of the spin rotation. For a give choice of p_g^{sp} for all p_g 's, the projective factor in Eq. (5) is determined by

$$p_g^{\text{sp}} p_{g'}^{\text{sp}} = \omega^{\text{sp}}(g, g') p_{gg'}^{\text{sp}}. \quad (9)$$

In our program, the information of p_g^{sp} and $\omega^{\text{sp}}(g, g')$ are stored, respectively, in `srg.dat` and `factor_system_spin.dat`.

3. Installation and usage

Here we explain how to install and use `qeirreps`. The flowchart of the calculations is shown in Fig. 2.

3.1. Compiling environment for `qeirreps`

A Fortran 90 compiler, BLAS, and LAPACK libraries are required for the installation of `qeirreps`. QUANTUM ESPRESSO must also be installed in advance. The version of QUANTUM ESPRESSO must be qe-6.3 or before.¹ To obtain old-formatted output files, QUANTUM ESPRESSO must be compiled with the following option:

```
$ ./configure --enable-xml=no .
```

In addition, the program `qe2respack` [66]² is required, which can be downloaded or cloned from the branch of `respack` “maxime2” in the GitHub repository (<https://github.com/mnmpdadish/respackDev/>). The program `qe2respack` is in the directory `util/qe2respack`. For installation, the file `Makefile` must be edited to specify the compiler, libraries, and the location of QUANTUM ESPRESSO in your compiling environment. By typing `$ make` in the directory `util/qe2respack`, the executable binary `qe2respack` is compiled.

¹This is because `qe2respack` does not support the later version of QUANTUM ESPRESSO. In future updates, we will propose our own interface between QUANTUM ESPRESSO and `qeirreps` instead of `qe2respack` to solve this limitation.

²This program `qe2respack` is the part of the program package `RESPACK` [66]. For the latest version of `RESPACK`, `qe2respack` does not support DFT calculations with spin-orbit coupling. For the usage of `qeirreps`, the specific version should be obtained as described in this section.

3.2. Installation of *qeirreps*

Our program `qeirreps` is released at GitHub (<https://github.com/qeirreps/qeirreps>). The program files which contain source files, documents, and examples can be cloned or downloaded from this repository. The file `qeirreps/src/Makefile` must be edited to specify the compiler and libraries in your compiling environment. By typing `$ make` in the source directory `qeirreps/src/`, the executable binary `qeirreps.x` is compiled.

3.3. Preparing input files of *qeirreps*

Our program `qeirreps` works based on the output of QUANTUM ESPRESSO. To prepare input files of `qeirreps`, the following three steps are needed to be done one by one:

1. Self-consistent first-principles (scf) calculation of a target material.
2. Non-self-consistent first-principles (nscf) calculation of the material for each high-symmetry momentum.
3. Data conversion from QUANTUM ESPRESSO output files to `qeirreps` input files.

The first two steps can be carried out by the standard functions of QUANTUM ESPRESSO. The result of the scf calculation is used in the successive nscf calculation. We refer to the directory that stores the wavefunction data computed by the nscf calculation `OUTDIR/PREFIX.save` below. For the moment, `qeirreps` requires norm-conserving calculations. Pseudo-potentials must be optimized for norm-conserving calculations (for example, Optimized Norm-Conserving Vanderbilt Pseudopotential [67] is available in PseudoDojo (<http://www.pseudo-dojo.org>) [68]) and the option `wf_collect` should be set `.TRUE.` in the input files for DFT calculations.

The output files in `OUTDIR/PREFIX.save` must be converted by `qe2respack` into the form of input files of `qeirreps`. To do this, a directory named `dir-wfn` must be created in advance in the work directory. The work directory is referred to as `DIRECTORY_NAME` here. Then, type the following in the work directory:

```
$ PATH_OF_qe2respack/qe2respack OUTDIR/PREFIX.save ,
```

where `PATH_OF_qe2respack` is the path to the directory `util/qe2respack`. `qeirreps` reads the files produced by `qe2respack` in the `dir-wfn` directory.

3.4. Running *qeirreps*

To run `qeirreps`, a directory named `output` must be created in the directory `DIRECTORY_NAME` above. Then type

```
$ PATH_OF_qeirreps/qeirreps.x DIRECTORY_NAME ,
```

where `PATH_OF_qeirreps` is the path to the directory `qeirreps/src`. There should be ten output files in `output`. Five of them named `*.dat` contain the following information: (i) the list of the point group part p_g in `pg.dat`, (ii) the list of the translation part t_g in `tg.dat`, (iii) the list of the spin rotation part p_g^{sp} in `srg.dat`, (iv) the factor system $\omega^{sp}(g, g')$ associated with the electronic spin in `factor_system_spin.dat`, and (v) the character tables of irreducible representations of Bloch wavefunctions in `character.dat`. Five of them named `*_import.txt` are the corresponding files for Mathematica usage. The standard output that appears during this calculation shows the lattice vectors, reciprocal lattice vectors, operation type of each symmetry operators, and so on.

For materials with inversion symmetry, `qeirreps` also implements the automatic evaluation of the \mathbb{Z}_4 index. To do this, an option of filling should be added to the command as

```
$ PATH_OF_qeirreps/qeirreps.x DIRECTORY_NAME FILLING.
```

Here, `FILLING` is the number of electrons per unit cell of the target material and is shown in the standard output of scf calculation by QUANTUM ESPRESSO as “`number of electrons = FILLING.`” Then, the program should generate an additional output named `z4.dat` that contains the value of the \mathbb{Z}_4 index.

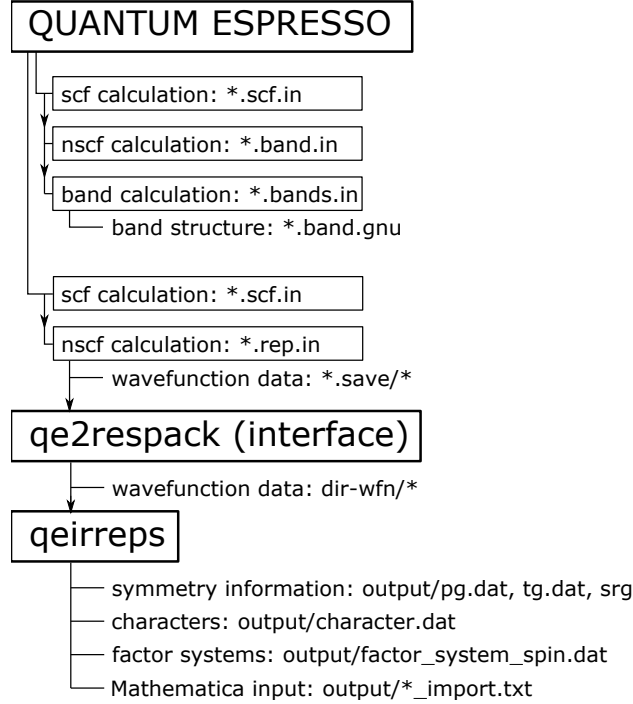


Figure 2: Flowchart of the process to calculate the representation characters of Bloch wavefunctions. The band structure and the wavefunctions of the target material are computed by QUANTUM ESPRESSO. These results are converted to the input files of `qeirreps` by `qe2respack`. Finally the representation characters are computed by `qeirreps`.

4. Examples

In this section, we discuss several examples to demonstrate the usage of `qeirreps`. We also explain how to compute topological indices based on the output of `qeirreps`.

4.1. Bismuth

Our first example is bismuth. The space group $R\bar{3}m$ (No.166) contains the inversion symmetry I . We obtain the crystal structure data of bismuth [Fig. 3 (a)] from Material Project [69] and converted it into the form of an input file for QUANTUM ESPRESSO (included in Appendix A.1) by SeeK-path [70, 71]³.

We compute the irreducible representations of wavefunctions by `qeirreps`, taking into account the spin-orbit coupling. Our results are shown in the band structure in Fig. 3 (b). The correspondence between the labels and characters of irreducible representations is included in Appendix B.1. These results are consistent with previous studies [47, 72].

³In this particular example, we manually shifted positions of atoms in the primitive unit cell so that we can compare our results with the one in Ref. [47]

We also compute the \mathbb{Z}_4 index [64, 65] using the option explained in Sec. 3.4. The output (z4.dat) shows

```
sum of parities for 8 k-points:
-7.999999999999963
z4 index:
2
```

Namely, the \mathbb{Z}_4 index for bismuth with the significant spin-orbit coupling is 2, indicating that this material is a higher-order topological insulator [73, 48, 47, 74]. The sample input files for bismuth are available in the directory `qeirreps/example`.

4.2. Silicon

To demonstrate that `qeirreps` equally works for nonsymmorphic space groups, let us discuss silicon. Its space group is $Fd\bar{3}m$ (No. 227), which also contains the inversion symmetry I . The calculation procedure is completely the same as those for bismuth in Sec. 4.1. Our results of irreducible representations are in Fig. 4 (b). The \mathbb{Z}_4 index is found to be zero. These results are consistent with the previous study in Ref. [47]. Sample programs for silicon are also in the directory `qeirreps/example`.

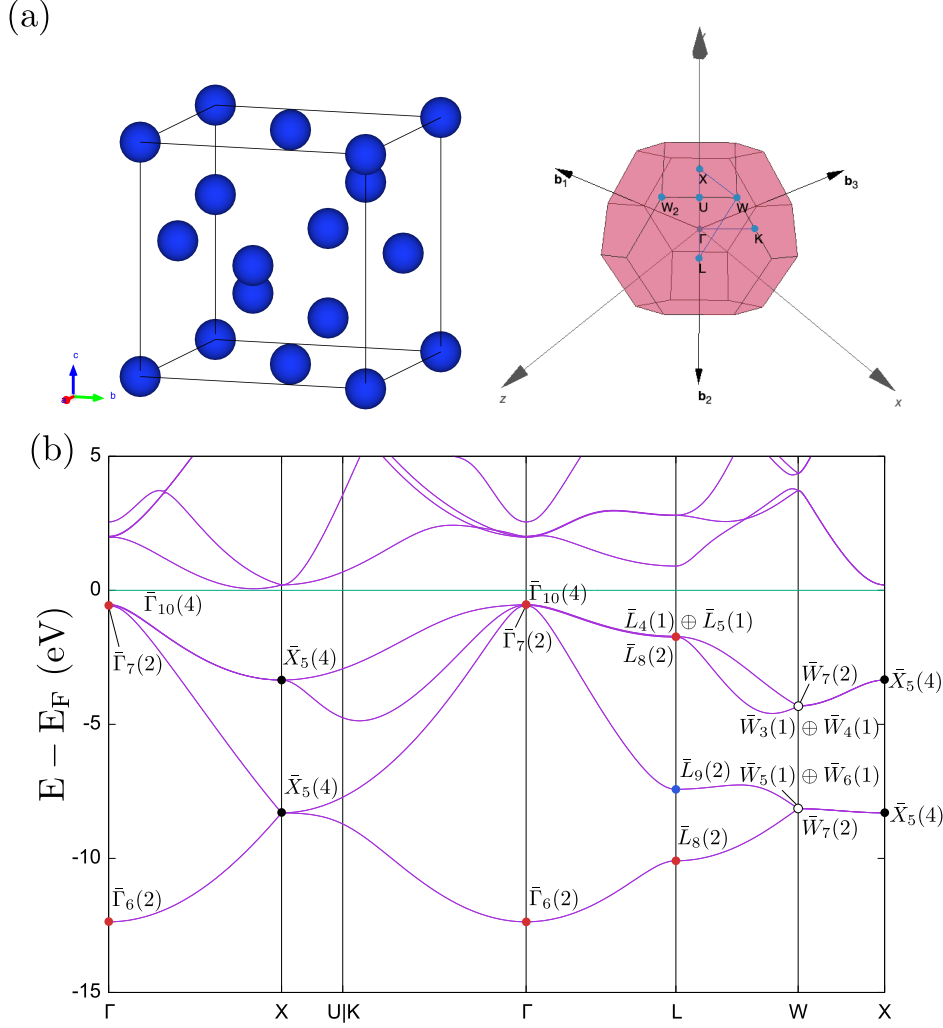


Figure 4: (a) The crystal structure [69] and the Brillouin zone [70, 71] of silicon. (b) The band structure of silicon with spin-orbit coupling. $\tilde{K}_\alpha(m)$ denotes a m -dimensional irreducible representation U_K^α at a high-symmetry point K . The correspondence between these labels and representation characters is included in Appendix B.3. The color of dots represents the inversion parity: when $\tilde{K}_\alpha(m)$ is marked red (blue), all m levels have the even (odd) parity, and when it is black, the half of them are even and the other half is odd. The little group at W does not have the inversion symmetry and open circles represent the absence of the inversion symmetry.

4.3. $PbPt_3$

As our third example, let us discuss $PbPt_3$, whose space group $Pm\bar{3}m$ (No. 221). This space group contains various elements such as the inversion (I), the rotoinversion about the z -axis (S_4^z), and the mirror symmetries. We also assume the time-reversal symmetry. Our results of irreducible representations in the presence of the spin-orbit coupling are in Fig. 5 (b).

In this symmetry settings, we can define a \mathbb{Z}_4 index (other than the sum of the inversion parities) and a

\mathbb{Z}_8 index by [75, 64, 65]

$$z_4 = \frac{3}{2}n_R^7 - \frac{3}{2}n_R^9 - \frac{1}{2}n_R^6 + \frac{1}{2}n_R^8 + n_R^{10} - n_R^{11} + \frac{3}{2}n_X^7 - \frac{3}{2}n_X^9 - \frac{1}{2}n_X^6 + \frac{1}{2}n_X^8 + n_M^6 + n_M^7 - n_M^8 - n_M^9 \pmod{4}, \quad (10)$$

$$z_8 = \frac{1}{4} \sum_{K \in \text{TRIMs}} \sum_{\alpha_K} \chi_K^{\alpha_K}(I) n_K^{\alpha_K} - \frac{1}{\sqrt{2}} \sum_{K' \in K_4} \sum_{\alpha_{K'}} \chi_{K'}^{\alpha_{K'}}(S_4^z) n_{K'}^{\alpha_{K'}} \pmod{8}, \quad (11)$$

where $n_K^{\alpha_K}$ represents the number of occupied states that have irreducible representations $U_K^{\alpha_K}$ of \mathcal{G}_K , and the set of $\{n_K^{\alpha_K}\}$ is included in [Appendix B.6](#). K_4 denotes four momenta invariant under the S_4^z . Although our program `qeirreps` does not offer an automated calculation of these indices, one can compute them manually using the output of our program. In this example, we find $(z_4, z_8) = (3, 6)$, which is consistent with Ref. [47]. According to Ref. [64, 65], these values indicate nontrivial mirror Chern numbers. Sample programs for PbPt_3 are included in `qeirreps/example`.

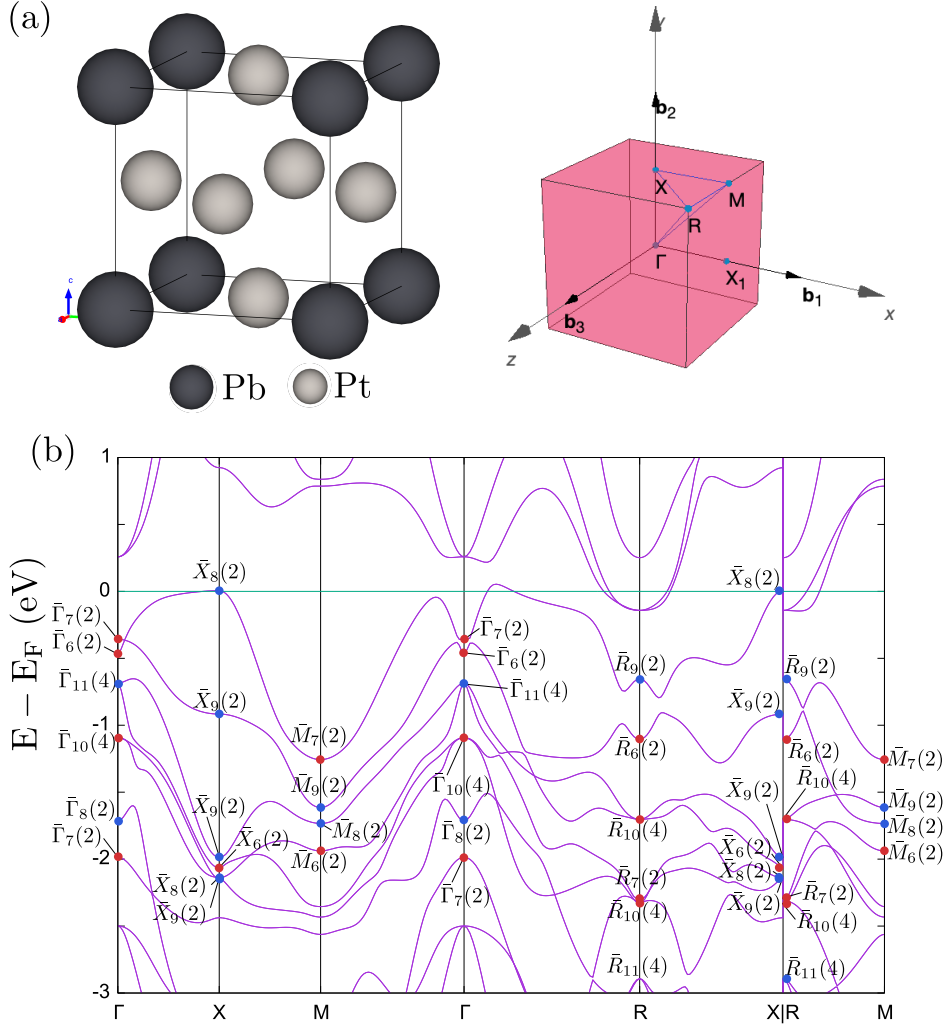


Figure 5: (a) The crystal structure [69] and the Brillouin zone [70, 71] of PbPt₃. (b) The band structure of PbPt₃ with spin-orbit coupling. $\bar{K}_\alpha(m)$ denotes a m -dimensional irreducible representation U_K^α at a high-symmetry point K . The correspondence between these labels and representation characters is included in Appendix B.5. The color of dots represents the inversion parity: when $\bar{K}_\alpha(m)$ is marked red (blue), all m levels have the even (odd) parity.

5. Conclusions

In conclusion, we developed a new open-source code `qeirreps` for computing irreducible representations in band structures based on the output of QUANTUM ESPRESSO. We explained the installation of the program and demonstrated its usage through examples. When combined with the symmetry indicator method, the output of this program can be used to diagnose the topological property of weakly interacting materials. Since QUANTUM ESPRESSO is a free, widely-used software, `qeirreps` should accelerate the exploration of new topological materials.

Acknowledgement

We would like to thank Ryotaro Arita and Motoaki Hirayama for fruitful discussions. All DFT calculations in this work has been done using the facilities of the Supercomputer Center, the Institute for Solid

State Physics, the University of Tokyo. The work of AM and SO is supported by Materials Education program for the future leaders in Research, Industry, and Technology (MERIT). SO is also supported by the ANRI Fellowship and JSPS KAKENHI Grant No. JP20J21692. The work of YN is supported by JSPS KAKENHI Grant No. 16H06345, 17K14336, 18H01158, 20K14423. The work of HW is supported by JSPS KAKENHI Grant No. JP17K17678 and by JST PRESTO Grant No. JPMJPR18LA.

Appendix A. Samples of Quantum ESPRESSO input

Appendix A.1. For the scf calculation of bismuth

```
&CONTROL
  calculation = 'scf'
  restart_mode='from_scratch',
  prefix='Bi'
  pseudo_dir='../..pseudo/soc/'
  outdir='./work/scf/'
  tstress=.true.
  tprnfor=.true.
  wf_collect=.true.
/
&SYSTEM
 ibrav = 0
  nat = 2
  ntyp = 1
  ecutwfc=100.
  occupations='smearing'
  smearing='m-p'
  degauss=0.01
  use_all_frac=.true.
  lspinorb=.true.
  noncolin=.true.
/
&ELECTRONS
  mixing_beta=0.3
  conv_thr=1.0d-8
/
ATOMIC_SPECIES
Bi      208.9804      Bi.upf
ATOMIC_POSITIONS angstrom
Bi  2.30479336  1.330673067  1.153637296
Bi -0.000000000 -0.000000000  2.838187257
K_POINTS automatic
8 8 8 0 0 0
CELL_PARAMETERS angstrom
  2.3047933600      1.3306730668      3.9918245533
 -2.3047933600      1.3306730668      3.9918245533
  0.0000000000     -2.6613461336      3.9918245533
```

Appendix A.2. For the nscf calculation of bismuth

```
&CONTROL
  calculation = 'bands'
  restart_mode='from_scratch',
  prefix='Bi'
  pseudo_dir='../..pseudo/soc/'
  outdir='./work/rep/'
  tstress=.true.
  tprnfor=.true.
  wf_collect=.true.
/
&SYSTEM
 ibrav = 0
  nat = 2
```

```

ntyp = 1
ecutwfc=100.
occupations='smearing'
smearing='m-p'
degauss=0.01
use_all_frac=.true.
lspinorb=.true.
noncolin=.true.
/
&ELECTRONS
  mixing_beta=0.3
  conv_thr=1.0d-8
/
ATOMIC_SPECIES
Bi      208.9804      Bi.upf
ATOMIC_POSITIONS angstrom
Bi  2.30479336  1.330673067  1.153637296
Bi  -0.00000000  -0.000000000  2.838187257
K_POINTS crystal
8
0.0    0.0    0.0    1
0.5    0.0    0.0    1
0.0    0.5    0.0    1
0.0    0.0    0.5    1
0.0    0.5    0.5    1
0.5    0.0    0.5    1
0.5    0.5    0.0    1
0.5    0.5    0.5    1
CELL_PARAMETERS angstrom
  2.3047933600    1.3306730668    3.9918245533
 -2.3047933600    1.3306730668    3.9918245533
  0.0000000000   -2.6613461336    3.9918245533

```

Appendix A.3. For the scf calculation of silicon

```

&CONTROL
  calculation = 'scf'
  restart_mode='from_scratch',
  prefix='Si'
  pseudo_dir='../..pseudo/soc'
  outdir='./work/scf/'
  tstress=.true.
  tprnfor=.true.
  wf_collect=.true.
/
&SYSTEM
  ibrav = 0
  nat = 2
  ntyp = 1
  ecutwfc=100.
  occupations='smearing'
  smearing='m-p'
  degauss=0.01
  use_all_frac=.true.
  lspinorb=.true.
  noncolin=.true.
/
&ELECTRONS
  mixing_beta=0.3
  conv_thr=1.0d-8
/
ATOMIC_SPECIES
Si      28.0855  Si.upf
ATOMIC_POSITIONS crystal
Si      0.625    0.625    0.625

```

```

Si          0.375      0.375      0.375
K_POINTS automatic
8 8 8 0 0 0
CELL_PARAMETERS angstrom
  0.0000000000      2.7347724300      2.7347724300
  2.7347724300      0.0000000000      2.7347724300
  2.7347724300      2.7347724300      0.0000000000

```

Appendix A.4. For the nscf calculation of silicon

```

&CONTROL
  calculation = 'bands'
  restart_mode='from_scratch',
  prefix='Si'
  pseudo_dir='../pseudo/soc'
  outdir='./work/rep/'
  tstress=.true.
  tprnfor=.true.
  wf_collect=.true.
/
&SYSTEM
  ibrav = 0
  nat = 2
  ntyp = 1
  ecutwfc=100.
  occupations='smearing'
  smearing='m-p'
  degauss=0.01
  use_all_frac=.true.
  lspinorb=.true.
  noncolin=.true.
/
&ELECTRONS
  mixing_beta=0.3
  conv_thr=1.0d-8
/
ATOMIC_SPECIES
Si      28.0855 Si.upf
ATOMIC_POSITIONS crystal
Si      0.625      0.625      0.625
Si      0.375      0.375      0.375
K_POINTS crystal
8
0.0      0.0      0.0      1
0.5      0.0      0.0      1
0.0      0.5      0.0      1
0.0      0.0      0.5      1
0.0      0.5      0.5      1
0.5      0.0      0.5      1
0.5      0.5      0.0      1
0.5      0.5      0.5      1
CELL_PARAMETERS angstrom
  0.0000000000      2.7347724300      2.7347724300
  2.7347724300      0.0000000000      2.7347724300
  2.7347724300      2.7347724300      0.0000000000

```

Appendix A.5. For the scf calculation of PbPt₃

```

&CONTROL
  calculation = 'scf'
  restart_mode='from_scratch',
  prefix='PbPt3'
  pseudo_dir='../pseudo/soc/'
  outdir='./work/scf'
  tstress=.true.
  tprnfor=.true.

```

```

    wf_collect=.true.
/
&SYSTEM
  ibrav = 0
  nat = 4
  ntyp = 2
  ecutwfc=100.
  occupations='smearing'
  smearing='m-p'
  degauss=0.01
  use_all_frac=.true.
  lspinorb=.true.
  noncolin=.true.
/
&ELECTRONS
  mixing_beta=0.3
  conv_thr=1.0d-8
/
ATOMIC_SPECIES
Pt      195.084 Pt.upf
Pb      207.2   Pb.upf
ATOMIC_POSITIONS angstrom
Pt      0.0000000000    2.0660527150    2.0660527150
Pt      2.0660527150    0.0000000000    2.0660527150
Pt      2.0660527150    2.0660527150    0.0000000000
Pb      0.0000000000    0.0000000000    0.0000000000
K_POINTS automatic
8 8 8 0 0 0
CELL_PARAMETERS angstrom
4.1321054300    0.0000000000    0.0000000000
0.0000000000    4.1321054300    0.0000000000
0.0000000000    0.0000000000    4.1321054300

```

Appendix A.6. For the nscf calculation of PbPt₃

```

&CONTROL
  calculation = 'bands'
  restart_mode='from_scratch',
  prefix='PbPt3'
  pseudo_dir='../..pseudo/soc/'
  outdir='./work/rep'
  tstress=.true.
  tprnfor=.true.
  wf_collect=.true.
/
&SYSTEM
  ibrav = 0
  nat = 4
  ntyp = 2
  ecutwfc=100.
  occupations='smearing'
  smearing='m-p'
  degauss=0.01
  use_all_frac=.true.
  lspinorb=.true.
  noncolin=.true.
/
&ELECTRONS
  mixing_beta=0.3
  conv_thr=1.0d-8
/
ATOMIC_SPECIES
Pt      195.084 Pt.upf
Pb      207.2   Pb.upf
ATOMIC_POSITIONS angstrom

```

```

Pt      0.0000000000    2.0660527150    2.0660527150
Pt      2.0660527150    0.0000000000    2.0660527150
Pt      2.0660527150    2.0660527150    0.0000000000
Pb      0.0000000000    0.0000000000    0.0000000000
K_POINTS crystal
8
0.0     0.0     0.0     1
0.5     0.0     0.0     1
0.0     0.5     0.0     1
0.0     0.0     0.5     1
0.0     0.5     0.5     1
0.5     0.0     0.5     1
0.5     0.5     0.0     1
0.5     0.5     0.5     1
CELL_PARAMETERS angstrom
4.1321054300    0.0000000000    0.0000000000
0.0000000000    4.1321054300    0.0000000000
0.0000000000    0.0000000000    4.1321054300

```

Appendix B. Information of irreducible representations

Appendix B.1. Character tables for bismuth

	Γ_4	Γ_5	Γ_6	Γ_7	Γ_8	Γ_9
1	1	1	1	1	2	2
3_{001}^+	-1	-1	-1	-1	1	1
3_{001}^-	-1	-1	-1	-1	1	1
2_{110}	$-i$	i	$-i$	i	0	0
2_{100}	i	$-i$	i	$-i$	0	0
2_{010}	$-i$	i	$-i$	i	0	0
I	1	1	-1	-1	2	-2
$I3_{001}^+$	-1	-1	1	1	1	-1
$I3_{001}^-$	-1	-1	1	1	1	-1
$I2_{110}$	$-i$	i	i	$-i$	0	0
$I2_{100}$	i	$-i$	$-i$	i	0	0
$I2_{010}$	$-i$	i	i	$-i$	0	0

	L_3	L_4	L_5	L_6
1	1	1	1	1
2_{110}	$-i$	i	$-i$	i
I	1	1	-1	-1
$I2_{110}$	$-i$	i	i	$-i$

	\bar{F}_3	\bar{F}_4	\bar{F}_5	\bar{F}_6
1	1	1	1	1
2_{110}	$-i$	i	$-i$	i
I	1	1	-1	-1
$I2_{110}$	$-i$	i	i	$-i$

	T_4	T_5	T_6	T_7	T_8	T_9
1	1	1	1	1	2	2
3_{001}^+	-1	-1	-1	-1	1	1
3_{001}^-	-1	-1	-1	-1	1	1
2_{110}	$-i$	i	$-i$	i	0	0
2_{100}	i	$-i$	i	$-i$	0	0
2_{010}	$-i$	i	$-i$	i	0	0
I	1	1	-1	-1	2	-2
$I3_{001}^+$	-1	-1	1	1	1	-1
$I3_{001}^-$	-1	-1	1	1	1	-1
$I2_{110}$	$-i$	i	i	$-i$	0	0
$I2_{100}$	i	$-i$	$-i$	i	0	0
$I2_{010}$	$-i$	i	i	$-i$	0	0

	H_3	H_4
1	1	1
2_{110}	$-i$	i

	M_3	M_4
1	1	1
m_{110}	$-i$	i

	S_3	S_4
1	1	1
2_{110}	$-i$	i

Appendix B.2. The number of irreducible representations for bismuth

ν	30
n_{Γ}^4	3
n_{Γ}^5	3
n_{Γ}^6	2
n_{Γ}^7	2
n_{Γ}^8	6
n_{Γ}^9	4
n_L^3	7
n_L^4	7
n_L^5	8
n_L^6	8
n_F^3	7
n_F^4	7
n_F^5	8
n_F^6	8
n_T^4	2
n_T^5	2
n_T^6	3
n_T^7	3
n_T^8	5
n_T^9	5

Appendix B.3. Character tables for silicon

	Γ_6	Γ_7	Γ_8	Γ_9	Γ_{10}	Γ_{11}
$\{1 0, 0, 0\}$	2	2	2	2	4	4
$\{2_{001} 0, 0, -1/2\}$	0	0	0	0	0	0
$\{2_{010} 0, -1/2, 0\}$	0	0	0	0	0	0
$\{2_{100} -1/2, 0, 0\}$	0	0	0	0	0	0
$\{3_{111}^+ 0, 0, 0\}$	1	1	1	1	-1	-1
$\{3_{111}^+ -1/2, 0, 0\}$	1	1	1	1	-1	-1
$\{3_{111}^+ 0, 0, -1/2\}$	1	1	1	1	-1	-1
$\{3_{111}^+ 0, -1/2, 0\}$	1	1	1	1	-1	-1
$\{3_{111}^- 0, 0, 0\}$	1	1	1	1	-1	-1
$\{3_{111}^- 0, -1/2, 0\}$	1	1	1	1	-1	-1
$\{3_{111}^- -1/2, 0, 0\}$	1	1	1	1	-1	-1
$\{3_{111}^- 0, 0, -1/2\}$	1	1	1	1	-1	-1
$\{2_{110} 0, 0, 1/2\}$	0	0	0	0	0	0
$\{2_{1\bar{1}0} 0, 0, 0\}$	0	0	0	0	0	0
$\{4_{001}^- 0, 1/2, 0\}$	$\sqrt{2}$	$-\sqrt{2}$	$\sqrt{2}$	$-\sqrt{2}$	0	0
$\{4_{001}^+ 1/2, 0, 0\}$	$\sqrt{2}$	$-\sqrt{2}$	$\sqrt{2}$	$-\sqrt{2}$	0	0
$\{4_{100}^- 0, 0, 1/2\}$	$\sqrt{2}$	$-\sqrt{2}$	$\sqrt{2}$	$-\sqrt{2}$	0	0
$\{2_{011}^- 1/2, 0, 0\}$	0	0	0	0	0	0
$\{2_{01\bar{1}}^- 0, 0, 0\}$	0	0	0	0	0	0
$\{4_{100}^+ 0, 1/2, 0\}$	$\sqrt{2}$	$-\sqrt{2}$	$\sqrt{2}$	$-\sqrt{2}$	0	0
$\{4_{010}^+ 0, 0, 1/2\}$	$\sqrt{2}$	$-\sqrt{2}$	$\sqrt{2}$	$-\sqrt{2}$	0	0
$\{2_{101}^- 0, 1/2, 0\}$	0	0	0	0	0	0
$\{4_{010}^- 1/2, 0, 0\}$	$\sqrt{2}$	$-\sqrt{2}$	$\sqrt{2}$	$-\sqrt{2}$	0	0
$\{2_{\bar{1}01}^- 0, 0, 0\}$	0	0	0	0	0	0
$\{I 0, 0, 0\}$	2	2	-2	-2	4	-4
$\{I2_{001} 0, 0, 1/2\}$	0	0	0	0	0	0
$\{I2_{010} 0, 1/2, 0\}$	0	0	0	0	0	0
$\{I2_{100} 1/2, 0, 0\}$	0	0	0	0	0	0
$\{I3_{111}^+ 0, 0, 0\}$	1	1	-1	-1	-1	1
$\{I3_{111}^+ 1/2, 0, 0\}$	1	1	-1	-1	-1	1
$\{I3_{111}^+ 0, 0, 1/2\}$	1	1	-1	-1	-1	1
$\{I3_{111}^+ 0, 1/2, 0\}$	1	1	-1	-1	-1	1
$\{I3_{111}^- 0, 0, 0\}$	1	1	-1	-1	-1	1
$\{I3_{111}^- 0, 1/2, 0\}$	1	1	-1	-1	-1	1
$\{I3_{111}^- 1/2, 0, 0\}$	1	1	-1	-1	-1	1
$\{I3_{111}^- 0, 0, 1/2\}$	1	1	-1	-1	-1	1
$\{I2_{110} 0, 0, -1/2\}$	0	0	0	0	0	0
$\{I2_{\bar{1}\bar{1}0} 0, 0, 0\}$	0	0	0	0	0	0
$\{I4_{001}^- 0, -1/2, 0\}$	$\sqrt{2}$	$-\sqrt{2}$	$-\sqrt{2}$	$\sqrt{2}$	0	0
$\{I4_{001}^+ -1/2, 0, 0\}$	$\sqrt{2}$	$-\sqrt{2}$	$-\sqrt{2}$	$\sqrt{2}$	0	0
$\{I4_{100}^- 0, 0, -1/2\}$	$\sqrt{2}$	$-\sqrt{2}$	$-\sqrt{2}$	$\sqrt{2}$	0	0
$\{I2_{011}^- -1/2, 0, 0\}$	0	0	0	0	0	0
$\{I2_{01\bar{1}}^- 0, 0, 0\}$	0	0	0	0	0	0
$\{I4_{100}^+ 0, -1/2, 0\}$	$\sqrt{2}$	$-\sqrt{2}$	$-\sqrt{2}$	$\sqrt{2}$	0	0
$\{I4_{010}^+ 0, 0, -1/2\}$	$\sqrt{2}$	$-\sqrt{2}$	$-\sqrt{2}$	$\sqrt{2}$	0	0
$\{I2_{101}^- 0, -1/2, 0\}$	0	0	0	0	0	0
$\{I4_{010}^- -1/2, 0, 0\}$	$\sqrt{2}$	$-\sqrt{2}$	$-\sqrt{2}$	$\sqrt{2}$	0	0
$\{I2_{\bar{1}01}^- 0, 0, 0\}$	0	0	0	0	0	0

	L_4	L_5	L_6	L_7	L_8	L_9
$\{1 0, 0, 0\}$	1	1	1	1	2	2
$\{3_{111}^+ 0, 0, 0\}$	-1	-1	-1	-1	1	1
$\{3_{111}^- 0, 0, 0\}$	-1	-1	-1	-1	1	1
$\{2_{1\bar{1}0} 0, 0, 0\}$	$-i$	i	$-i$	i	0	0
$\{2_{01\bar{1}} 0, 0, 0\}$	$-i$	i	$-i$	i	0	0
$\{2_{\bar{1}01} 0, 0, 0\}$	$-i$	i	$-i$	i	0	0
$\{I 0, 0, 0\}$	1	1	-1	-1	2	-2
$\{I3_{111}^+ 0, 0, 0\}$	-1	-1	1	1	1	-1
$\{I3_{111}^- 0, 0, 0\}$	-1	-1	1	1	1	-1
$\{I2_{1\bar{1}0} 0, 0, 0\}$	$-i$	i	i	$-i$	0	0
$\{I2_{01\bar{1}} 0, 0, 0\}$	$-i$	i	i	$-i$	0	0
$\{I2_{\bar{1}01} 0, 0, 0\}$	$-i$	i	i	$-i$	0	0

	X_5
$\{1 0, 0, 0\}$	4
$\{2_{001} 0, 0, -1/2\}$	0
$\{2_{010} 0, -1/2, 0\}$	0
$\{2_{100} -1/2, 0, 0\}$	0
$\{4_{010}^+ 0, 0, 1/2\}$	0
$\{2_{101} 0, 1/2, 0\}$	0
$\{4_{010}^- 1/2, 0, 0\}$	0
$\{2_{\bar{1}01} 0, 0, 0\}$	0
$\{I 0, 0, 0\}$	0
$\{I2_{001} 0, 0, 1/2\}$	0
$\{I2_{010} 0, 1/2, 0\}$	0
$\{I2_{100} 1/2, 0, 0\}$	0
$\{I4_{010}^+ 0, 0, -1/2\}$	0
$\{I2_{101} 0, -1/2, 0\}$	0
$\{I4_{010}^- -1/2, 0, 0\}$	0
$\{I2_{\bar{1}01} 0, 0, 0\}$	0

	W_3	W_4	W_5	W_6	W_7
$\{1 0, 0, 0\}$	1	1	1	1	2
$\{2_{100} -1/2, 0, 0\}$	$-i$	$-i$	$-i$	$-i$	$2i$
$\{2_{011} 1/2, 0, 0\}$	1	-1	1	-1	0
$\{2_{01\bar{1}} 0, 0, 0\}$	i	$-i$	i	$-i$	0
$\{I2_{001} 0, 0, 1/2\}$	$e^{i\pi/4}$	$e^{-i3\pi/4}$	$e^{-i3\pi/4}$	$e^{i\pi/4}$	0
$\{I2_{010} 0, 1/2, 0\}$	$e^{-i\pi/4}$	$e^{i3\pi/4}$	$e^{i3\pi/4}$	$e^{-i\pi/4}$	0
$\{I4_{100}^- 0, 0, -1/2\}$	$e^{i3\pi/4}$	$e^{i3\pi/4}$	$e^{-i\pi/4}$	$e^{-i\pi/4}$	0
$\{I4_{100}^+ 0, -1/2, 0\}$	$e^{-i3\pi/4}$	$e^{-i3\pi/4}$	$e^{i\pi/4}$	$e^{i\pi/4}$	0

	K_5
$\{1 0, 0, 0\}$	2
$\{2_{100} - 1/2, 0, 0\}$	0
$\{I2_{001} 0, 0, 1/2\}$	0
$\{I2_{1\bar{1}0} 0, 0, 0\}$	0

Appendix B.4. Irreducible representations of silicon

ν	8
n_{Γ}^6	1
n_{Γ}^7	1
n_{Γ}^8	0
n_{Γ}^9	0
n_{Γ}^{10}	1
n_{Γ}^{11}	0
n_L^4	1
n_L^5	1
n_L^6	0
n_L^7	0
n_L^8	2
n_L^9	1
n_W^3	1
n_W^4	1
n_W^5	1
n_W^6	1
n_W^7	2

Appendix B.5. Character table for $PbPt_3$

	Γ_6	Γ_7	Γ_8	Γ_9	Γ_{10}	Γ_{11}
1	2	2	2	2	4	4
2_{001}	0	0	0	0	0	0
2_{010}	0	0	0	0	0	0
2_{100}	0	0	0	0	0	0
3_{111}^+	1	1	1	1	-1	-1
$3_{11\bar{1}}^+$	1	1	1	1	-1	-1
$3_{\bar{1}\bar{1}\bar{1}}^+$	1	1	1	1	-1	-1
$3_{\bar{1}\bar{1}1}^+$	1	1	1	1	-1	-1
3_{111}^-	1	1	1	1	-1	-1
$3_{11\bar{1}}^-$	1	1	1	1	-1	-1
$3_{\bar{1}\bar{1}\bar{1}}^-$	1	1	1	1	-1	-1
$3_{\bar{1}\bar{1}1}^-$	1	1	1	1	-1	-1
2_{110}	0	0	0	0	0	0
$2_{1\bar{1}0}$	0	0	0	0	0	0
4_{001}^+	$\sqrt{2}$	$-\sqrt{2}$	$\sqrt{2}$	$-\sqrt{2}$	0	0
4_{001}^-	$\sqrt{2}$	$-\sqrt{2}$	$\sqrt{2}$	$-\sqrt{2}$	0	0
4_{100}^+	$\sqrt{2}$	$-\sqrt{2}$	$\sqrt{2}$	$-\sqrt{2}$	0	0
4_{100}^-	$\sqrt{2}$	$-\sqrt{2}$	$\sqrt{2}$	$-\sqrt{2}$	0	0
2_{011}	0	0	0	0	0	0
$2_{01\bar{1}}$	0	0	0	0	0	0
4_{100}^+	$\sqrt{2}$	$-\sqrt{2}$	$\sqrt{2}$	$-\sqrt{2}$	0	0
4_{010}^+	$\sqrt{2}$	$-\sqrt{2}$	$\sqrt{2}$	$-\sqrt{2}$	0	0
2_{101}	0	0	0	0	0	0
$4_{\bar{0}10}^-$	$\sqrt{2}$	$-\sqrt{2}$	$\sqrt{2}$	$-\sqrt{2}$	0	0
$2_{\bar{1}01}$	0	0	0	0	0	0
I	2	2	-2	-2	4	-4
$I2_{001}$	0	0	0	0	0	0
$I2_{010}$	0	0	0	0	0	0
$I2_{100}$	0	0	0	0	0	0
$I3_{111}^+$	1	1	-1	-1	-1	1
$I3_{11\bar{1}}^+$	1	1	-1	-1	-1	1
$I3_{\bar{1}\bar{1}\bar{1}}^+$	1	1	-1	-1	-1	1
$I3_{\bar{1}\bar{1}1}^+$	1	1	-1	-1	-1	1
$I3_{111}^-$	1	1	-1	-1	-1	1
$I3_{11\bar{1}}^-$	1	1	-1	-1	-1	1
$I3_{\bar{1}\bar{1}\bar{1}}^-$	1	1	-1	-1	-1	1
$I3_{\bar{1}\bar{1}1}^-$	1	1	-1	-1	-1	1
$I2_{110}$	0	0	0	0	0	0
$I2_{1\bar{1}0}$	0	0	0	0	0	0
$I4_{001}^-$	$\sqrt{2}$	$-\sqrt{2}$	$-\sqrt{2}$	$\sqrt{2}$	0	0
$I4_{001}^+$	$\sqrt{2}$	$-\sqrt{2}$	$-\sqrt{2}$	$\sqrt{2}$	0	0
$I4_{100}^-$	$\sqrt{2}$	$-\sqrt{2}$	$-\sqrt{2}$	$\sqrt{2}$	0	0
$I2_{011}$	0	0	0	0	0	0
$I2_{01\bar{1}}$	0	0	0	0	0	0
$I4_{100}^+$	$\sqrt{2}$	$-\sqrt{2}$	$-\sqrt{2}$	$\sqrt{2}$	0	0
$I4_{010}^+$	$\sqrt{2}$	$-\sqrt{2}$	$-\sqrt{2}$	$\sqrt{2}$	0	0
$I2_{101}$	0	0	0	0	0	0
$I4_{\bar{0}10}^-$	$\sqrt{2}$	$-\sqrt{2}$	$-\sqrt{2}$	$\sqrt{2}$	0	0
$I2_{\bar{1}01}$	0	0	0	0	0	0

	M_6	M_7	M_8	M_9
1	2	2	2	2
2_{001}	0	0	0	0
2_{010}	0	0	0	0
2_{100}	0	0	0	0
2_{110}	0	0	0	0
$2_{1\bar{1}0}$	0	0	0	0
4_{001}^-	$-\sqrt{2}$	$\sqrt{2}$	$-\sqrt{2}$	$\sqrt{2}$
4_{001}^+	$-\sqrt{2}$	$\sqrt{2}$	$-\sqrt{2}$	$\sqrt{2}$
I	2	2	-2	-2
$I2_{001}$	0	0	0	0
$I2_{010}$	0	0	0	0
$I2_{100}$	0	0	0	0
$I2_{110}$	0	0	0	0
$I2_{1\bar{1}0}$	0	0	0	0
$I4_{001}^-$	$-\sqrt{2}$	$\sqrt{2}$	$\sqrt{2}$	$-\sqrt{2}$
$I4_{001}^+$	$-\sqrt{2}$	$\sqrt{2}$	$\sqrt{2}$	$-\sqrt{2}$

	R_6	R_7	R_8	R_9	R_{10}	R_{11}
1	2	2	2	2	4	4
2_{001}	0	0	0	0	0	0
2_{010}	0	0	0	0	0	0
2_{100}	0	0	0	0	0	0
3_{111}^+	1	1	1	1	-1	-1
$3_{1\bar{1}\bar{1}}^+$	1	1	1	1	-1	-1
$3_{1\bar{1}\bar{1}}^+$	1	1	1	1	-1	-1
$3_{\bar{1}\bar{1}\bar{1}}^+$	1	1	1	1	-1	-1
3_{111}^-	1	1	1	1	-1	-1
$3_{1\bar{1}\bar{1}}^-$	1	1	1	1	-1	-1
$3_{\bar{1}\bar{1}\bar{1}}^-$	1	1	1	1	-1	-1
$3_{\bar{1}\bar{1}\bar{1}}^-$	1	1	1	1	-1	-1
2_{110}	0	0	0	0	0	0
$2_{1\bar{1}0}$	0	0	0	0	0	0
4_{001}^-	$\sqrt{2}$	$-\sqrt{2}$	$\sqrt{2}$	$-\sqrt{2}$	0	0
4_{001}^+	$\sqrt{2}$	$-\sqrt{2}$	$\sqrt{2}$	$-\sqrt{2}$	0	0
4_{100}^-	$\sqrt{2}$	$-\sqrt{2}$	$\sqrt{2}$	$-\sqrt{2}$	0	0
2_{011}	0	0	0	0	0	0
$2_{01\bar{1}}$	0	0	0	0	0	0
4_{100}^+	$\sqrt{2}$	$-\sqrt{2}$	$\sqrt{2}$	$-\sqrt{2}$	0	0
4_{010}^+	$\sqrt{2}$	$-\sqrt{2}$	$\sqrt{2}$	$-\sqrt{2}$	0	0
2_{101}	0	0	0	0	0	0
4_{010}^-	$\sqrt{2}$	$-\sqrt{2}$	$\sqrt{2}$	$-\sqrt{2}$	0	0
$2_{\bar{1}01}$	0	0	0	0	0	0
I	2	2	-2	-2	4	-4
$I2_{001}$	0	0	0	0	0	0
$I2_{010}$	0	0	0	0	0	0
$I2_{100}$	0	0	0	0	0	0
$I3_{111}^+$	1	1	-1	-1	-1	1
$I3_{1\bar{1}\bar{1}}^+$	1	1	-1	-1	-1	1
$I3_{1\bar{1}\bar{1}}^+$	1	1	-1	-1	-1	1
$I3_{\bar{1}\bar{1}\bar{1}}^+$	1	1	-1	-1	-1	1
$I3_{111}^-$	1	1	-1	-1	-1	1
$I3_{1\bar{1}\bar{1}}^-$	1	1	-1	-1	-1	1
$I3_{\bar{1}\bar{1}\bar{1}}^-$	1	1	-1	-1	-1	1
$I3_{\bar{1}\bar{1}\bar{1}}^-$	1	1	-1	-1	-1	1
$I2_{110}$	0	0	0	0	0	0
$I2_{1\bar{1}0}$	0	0	0	0	0	0
$I4_{001}^-$	$\sqrt{2}$	$-\sqrt{2}$	$-\sqrt{2}$	$\sqrt{2}$	0	0
$I4_{001}^+$	$\sqrt{2}$	$-\sqrt{2}$	$-\sqrt{2}$	$\sqrt{2}$	0	0
$I4_{100}^-$	$\sqrt{2}$	$-\sqrt{2}$	$-\sqrt{2}$	$\sqrt{2}$	0	0
$I2_{011}$	0	0	0	0	0	0
$I2_{01\bar{1}}$	0	0	0	0	0	0
$I4_{100}^+$	$\sqrt{2}$	$-\sqrt{2}$	$-\sqrt{2}$	$\sqrt{2}$	0	0
$I4_{010}^+$	$\sqrt{2}$	$-\sqrt{2}$	$-\sqrt{2}$	$\sqrt{2}$	0	0
$I2_{101}$	0	0	0	0	0	0
$I4_{010}^-$	$\sqrt{2}$	$-\sqrt{2}$	$-\sqrt{2}$	$\sqrt{2}$	0	0
$I2_{\bar{1}01}$	0	0	0	0	0	0

	X_6	X_7	X_8	X_9
1	2	2	2	2
2_{001}	0	0	0	0
2_{010}	0	0	0	0
2_{100}	0	0	0	0
4_{010}^+	$\sqrt{2}$	$-\sqrt{2}$	$\sqrt{2}$	$-\sqrt{2}$
2_{101}	0	0	0	0
4_{010}^-	$\sqrt{2}$	$-\sqrt{2}$	$\sqrt{2}$	$-\sqrt{2}$
$2_{\bar{1}01}$	0	0	0	0
I	2	2	-2	-2
$I2_{001}$	0	0	0	0
$I2_{010}$	0	0	0	0
$I2_{100}$	0	0	0	0
$I4_{010}^+$	$\sqrt{2}$	$-\sqrt{2}$	$-\sqrt{2}$	$\sqrt{2}$
$I2_{101}$	0	0	0	0
$I4_{010}^-$	$\sqrt{2}$	$-\sqrt{2}$	$-\sqrt{2}$	$\sqrt{2}$
$I2_{\bar{1}01}$	0	0	0	0

Appendix B.6. Irreducible representations of $PbPt_3$

ν	68
n_{Γ}^6	4
n_{Γ}^7	4
n_{Γ}^8	3
n_{Γ}^9	1
n_{Γ}^{10}	7
n_{Γ}^{11}	4
n_M^6	10
n_M^7	9
n_M^8	8
n_M^9	7
n_R^6	3
n_R^7	4
n_R^8	2
n_R^9	3
n_R^{10}	7
n_R^{11}	4
n_X^6	9
n_X^7	9
n_X^8	9
n_X^9	7

References

- [1] W. Kohn and L. J. Sham, *Phys. Rev.* **140**, A1133 (1965).
- [2] C. L. Kane and E. J. Mele, *Phys. Rev. Lett.* **95**, 146802 (2005).
- [3] C. L. Kane and E. J. Mele, *Phys. Rev. Lett.* **95**, 226801 (2005).
- [4] B. A. Bernevig, T. L. Hughes, and S.-C. Zhang, *Science* **314**, 1757 (2006).

- [5] M. König, S. Wiedmann, C. Brüne, A. Roth, H. Buhmann, L. W. Molenkamp, X.-L. Qi, and S.-C. Zhang, *Science* **318**, 766 (2007).
- [6] L. Fu and C. L. Kane, *Phys. Rev. B* **74**, 195312 (2006).
- [7] L. Fu, C. L. Kane, and E. J. Mele, *Phys. Rev. Lett.* **98**, 106803 (2007).
- [8] J. E. Moore and L. Balents, *Phys. Rev. B* **75**, 121306 (2007).
- [9] L. Fu and C. L. Kane, *Phys. Rev. B* **76**, 045302 (2007).
- [10] D. Hsieh, D. Qian, L. Wray, Y. Xia, Y. S. Hor, R. J. Cava, and M. Z. Hasan, *Nature* **452**, 970 (2008).
- [11] C. Liu, T. L. Hughes, X.-L. Qi, K. Wang, and S.-C. Zhang, *Phys. Rev. Lett.* **100**, 236601 (2008).
- [12] X.-L. Qi, T. L. Hughes, and S.-C. Zhang, *Phys. Rev. B* **78**, 195424 (2008).
- [13] D. Hsieh, Y. Xia, D. Qian, L. Wray, J. H. Dil, F. Meier, J. Osterwalder, L. Patthey, J. G. Checkelsky, N. P. Ong, A. V. Fedorov, H. Lin, A. Bansil, D. Grauer, Y. S. Hor, R. J. Cava, and M. Z. Hasan, *Nature* **460**, 1101 (2009).
- [14] Y. Xia, D. Qian, D. Hsieh, L. Wray, A. Pal, H. Lin, A. Bansil, D. Grauer, Y. S. Hor, R. J. Cava, and M. Z. Hasan, *Nature Physics* **5**, 398 (2009).
- [15] R. Roy, *Phys. Rev. B* **79**, 195322 (2009).
- [16] R. Yu, W. Zhang, H.-J. Zhang, S.-C. Zhang, X. Dai, and Z. Fang, *Science* **329**, 61 (2010).
- [17] I. Knez, R.-R. Du, and G. Sullivan, *Phys. Rev. Lett.* **107**, 136603 (2011).
- [18] C.-Z. Chang, J. Zhang, X. Feng, J. Shen, Z. Zhang, M. Guo, K. Li, Y. Ou, P. Wei, L.-L. Wang, Z.-Q. Ji, Y. Feng, S. Ji, X. Chen, J. Jia, X. Dai, Z. Fang, S.-C. Zhang, K. He, Y. Wang, L. Lu, X.-C. Ma, and Q.-K. Xue, *Science* **340**, 167 (2013).
- [19] A. P. Schnyder, S. Ryu, A. Furusaki, and A. W. W. Ludwig, *Phys. Rev. B* **78**, 195125 (2008).
- [20] A. Kitaev, *AIP Conference Proceedings* **1134**, 22 (2009).
- [21] S. Ryu, A. P. Schnyder, A. Furusaki, and A. W. W. Ludwig, *New Journal of Physics* **12**, 065010 (2010).
- [22] D. S. Freed and G. W. Moore, *Annales Henri Poincaré* **14**, 1927 (2013).
- [23] H. Song, S.-J. Huang, L. Fu, and M. Hermele, *Phys. Rev. X* **7**, 011020 (2017).
- [24] J. Kruthoff, J. de Boer, J. van Wezel, C. L. Kane, and R.-J. Slager, *Phys. Rev. X* **7**, 041069 (2017).
- [25] R. Thorngren and D. V. Else, *Phys. Rev. X* **8**, 011040 (2018).
- [26] S.-J. Huang, H. Song, Y.-P. Huang, and M. Hermele, *Phys. Rev. B* **96**, 205106 (2017).
- [27] K. Shiozaki, M. Sato, and K. Gomi, [arXiv:1802.06694](https://arxiv.org/abs/1802.06694).
- [28] Z. Song, S.-J. Huang, Y. Qi, C. Fang, and M. Hermele, [arXiv:1810.02330](https://arxiv.org/abs/1810.02330).
- [29] Y. Tanaka, Z. Ren, T. Sato, K. Nakayama, S. Souma, T. Takahashi, K. Segawa, and Y. Ando, *Nature Physics* **8**, 800 (2012).
- [30] T. H. Hsieh, H. Lin, J. Liu, W. Duan, A. Bansil, and L. Fu, *Nature Communications* **3**, 982 (2012).
- [31] F. Schindler, A. M. Cook, M. G. Vergniory, Z. Wang, S. S. P. Parkin, B. A. Bernevig, and T. Neupert, *Science Advances* **4**, eaat0346 (2018).
- [32] Z. Song, Z. Fang, and C. Fang, *Phys. Rev. Lett.* **119**, 246402 (2017).
- [33] W. A. Benalcazar, B. A. Bernevig, and T. L. Hughes, *Science* **357**, 61 (2017).
- [34] W. A. Benalcazar, B. A. Bernevig, and T. L. Hughes, *Phys. Rev. B* **96**, 245115 (2017).
- [35] A. Matsugatani and H. Watanabe, *Phys. Rev. B* **98**, 205129 (2018).
- [36] L. Trifunovic and P. W. Brouwer, *Phys. Rev. X* **9**, 011012 (2019).
- [37] C. Fang and L. Fu, *Science Advances* **5**, eaat2374 (2019).
- [38] S. M. Young, S. Zaheer, J. C. Y. Teo, C. L. Kane, E. J. Mele, and A. M. Rappe, *Phys. Rev. Lett.* **108**, 140405 (2012).
- [39] X. Wan, A. M. Turner, A. Vishwanath, and S. Y. Savrasov, *Phys. Rev. B* **83**, 205101 (2011).
- [40] Z. Wang, A. Alexandradinata, R. J. Cava, and B. A. Bernevig, *Nature* **532**, 189 (2016).
- [41] K. Shiozaki, M. Sato, and K. Gomi, *Phys. Rev. B* **91**, 155120 (2015).
- [42] C. Fang and L. Fu, *Phys. Rev. B* **91**, 161105 (2015).
- [43] H. C. Po, A. Vishwanath, and H. Watanabe, *Nat. Commun.* **8**, 50 (2017).
- [44] F. Tang, H. C. Po, A. Vishwanath, and X. Wan, *Nat. Phys.* **15**, 470 (2019).
- [45] F. Tang, H. C. Po, A. Vishwanath, and X. Wan, *Sci. Adv.* **5** (2019).
- [46] T. Zhang, Y. Jiang, Z. Song, H. Huang, Y. He, Z. Fang, H. Weng, and C. Fang, *Nature* **566**, 475 (2019).
- [47] M. G. Vergniory, L. Elcoro, C. Felser, N. Regnault, B. A. Bernevig, and Z. Wang, *Nature* **566**, 480 (2019).
- [48] F. Tang, H. C. Po, A. Vishwanath, and X. Wan, *Nature* **566**, 486 (2019).
- [49] H. Watanabe, H. C. Po, and A. Vishwanath, *Sci. Adv.* **4**, eaat8685 (2018).
- [50] S. Ono and H. Watanabe, *Phys. Rev. B* **98**, 115150 (2018).
- [51] S. Ono, Y. Yanase, and H. Watanabe, *Phys. Rev. Res.* **1**, 013012 (2019).
- [52] A. Skurativska, T. Neupert, and M. H. Fischer, *Phys. Rev. Research* **2**, 013064 (2020).
- [53] K. Shiozaki, [arXiv:1907.13632](https://arxiv.org/abs/1907.13632).
- [54] S. Ono, H. C. Po, and H. Watanabe, *Science Advances* **6**, eaaz8367 (2020).
- [55] M. Geier, P. W. Brouwer, and L. Trifunovic, (2019), [arXiv:1910.11271](https://arxiv.org/abs/1910.11271).
- [56] J. Gao, Q. Wu, C. Persson, and Z. Wang, “Irvsp: to obtain irreducible representations of electronic states in the VASP,” (2020), [arXiv:2002.04032](https://arxiv.org/abs/2002.04032).
- [57] P. Blaha, K. Schwarz, G. K. H. Madsen, D. Kvasnicka, and J. Luitz, [WIEN2K, An Augmented Plane Wave + Local Orbitals Program for Calculating Crystal Properties](https://www.tuwien.at/en/technik/wien2k) (Karlheinz Schwarz, Techn. Universität Wien, Austria, 2001).
- [58] G. Kresse and J. Furthmüller, *Phys. Rev. B* **54**, 11169 (1996).
- [59] P. Giannozzi, S. Baroni, N. Bonini, M. Calandra, R. Car, C. Cavazzoni, D. Ceresoli, G. L. Chiarotti, M. Cococcioni, I. Dabo, A. D. Corso, S. de Gironcoli, S. Fabris, G. Fratesi, R. Gebauer, U. Gerstmann, C. Gougoussis, A. Kokalj, M. Lazzeri,

- L. Martin-Samos, N. Marzari, F. Mauri, R. Mazzarello, S. Paolini, A. Pasquarello, L. Paulatto, C. Sbraccia, S. Scandolo, G. Scლაუzero, A. P. Seitsonen, A. Smogunov, P. Umari, and R. M. Wentzcovitch, *Journal of Physics: Condensed Matter* **21**, 395502 (2009).
- [60] P. Giannozzi, O. Andreussi, T. Brumme, O. Bunau, M. B. Nardelli, M. Calandra, R. Car, C. Cavazzoni, D. Ceresoli, M. Cococcioni, N. Colonna, I. Carnimeo, A. D. Corso, S. de Gironcoli, P. Delugas, R. A. DiStasio, A. Ferretti, A. Floris, G. Fratesi, G. Fugallo, R. Gebauer, U. Gerstmann, F. Giustino, T. Gorni, J. Jia, M. Kawamura, H.-Y. Ko, A. Kokalj, E. Küçükbenli, M. Lazzeri, M. Marsili, N. Marzari, F. Mauri, N. L. Nguyen, H.-V. Nguyen, A. O. de-la Roza, L. Paulatto, S. Poncé, D. Rocca, R. Sabatini, B. Santra, M. Schlipf, A. P. Seitsonen, A. Smogunov, I. Timrov, T. Thonhauser, P. Umari, N. Vast, X. Wu, and S. Baroni, *Journal of Physics: Condensed Matter* **29**, 465901 (2017).
- [61] C. J. Bradley and A. P. Cracknell, *The Mathematical Theory of Symmetry in Solids* (Oxford University Press, 1972).
- [62] H. C. Po, *Journal of Physics: Condensed Matter* **32**, 263001 (2020).
- [63] Z. Song, T. Zhang, and C. Fang, *Phys. Rev. X* **8**, 031069 (2018).
- [64] E. Khalaf, H. C. Po, A. Vishwanath, and H. Watanabe, *Phys. Rev. X* **8**, 031070 (2018).
- [65] Z. Song, T. Zhang, Z. Fang, and C. Fang, *Nat. Commun.* **9**, 3530 (2018).
- [66] K. Nakamura, Y. Yoshimoto, Y. Nomura, T. Tadano, M. Kawamura, T. Kosugi, K. Yoshimi, T. Misawa, and Y. Motoyama, arXiv preprint arXiv:2001.02351 (2020).
- [67] D. R. Hamann, *Phys. Rev. B* **88**, 085117 (2013).
- [68] M. [van Setten], M. Giantomassi, E. Bousquet, M. Verstraete, D. Hamann, X. Gonze, and G.-M. Rignanese, *Computer Physics Communications* **226**, 39 (2018).
- [69] A. Jain, S. P. Ong, G. Hautier, W. Chen, W. D. Richards, S. Dacek, S. Cholia, D. Gunter, D. Skinner, G. Ceder, and K. a. Persson, *APL Materials* **1**, 011002 (2013).
- [70] Y. Hinuma, G. Pizzi, Y. Kumagai, F. Oba, and I. Tanaka, *Computational Materials Science* **128**, 140 (2017).
- [71] A. Togo and I. Tanaka, arXiv preprint arXiv:1808.01590 (2018).
- [72] L. Elcoro, B. Bradlyn, Z. Wang, M. G. Vergniory, J. Cano, C. Felser, B. A. Bernevig, D. Orobengoa, G. de la Flor, and M. I. Aroyo, *Journal of Applied Crystallography* **50**, 1457 (2017).
- [73] F. Schindler, Z. Wang, M. G. Vergniory, A. M. Cook, A. Murani, S. Sengupta, A. Y. Kasumov, R. Deblock, S. Jeon, I. Drozdov, H. Bouchiat, S. Guéron, A. Yazdani, B. A. Bernevig, and T. Neupert, *Nature Physics* **14**, 918 (2018).
- [74] C.-H. Hsu, X. Zhou, T.-R. Chang, Q. Ma, N. Gedik, A. Bansil, S.-Y. Xu, H. Lin, and L. Fu, *Proceedings of the National Academy of Sciences* **116**, 13255 (2019).
- [75] C. Fang, M. J. Gilbert, and B. A. Bernevig, *Phys. Rev. B* **86**, 115112 (2012).